An attempt to generate mechanical white etching layer on rail surface on a new rolling contact test bench

Pierrick Merino, Sophie Cazottes, Vincent Lafile, Marion Risbet, Aurelien Saulot, Salima Bouvier, Julie Marteau, Yves Berthier

▶ **To cite this version:**

Pierrick Merino, Sophie Cazottes, Vincent Lafile, Marion Risbet, Aurelien Saulot, et al.. An attempt to generate mechanical white etching layer on rail surface on a new rolling contact test bench. Wear, 2021, 482, 10.1016/j.wear.2021.203945 . hal-03484906

HAL Id: hal-03484906
https://hal.science/hal-03484906

Submitted on 13 Jun 2023

HAL is a multi-disciplinary open access archive for the deposit and dissemination of scientific research documents, whether they are published or not. The documents may come from teaching and research institutions in France or abroad, or from public or private research centers.

L'archive ouverte pluridisciplinaire **HAL**, est destinée au dépôt et à la diffusion de documents scientifiques de niveau recherche, publiés ou non, émanant des établissements d'enseignement et de recherche français ou étrangers, des laboratoires publics ou privés.

Distributed under a Creative Commons Attribution - NonCommercial 4.0 International License

Version of Record: https://www.sciencedirect.com/science/article/pii/S0043164821003343
Manuscript_9a22d5f0fac493b48e48a233705856e1

Title: How to reproduce a mechanical white etching layer (WEL) on rail surface thanks to a new experimental wheel-rail contact test bench

Authors

Pierrick Merino[a], Sophie Cazottes[b], Vincent Lafilée[c], Marion Risbet[c], Aurélien Saulot[a], Salima Bouvier[c], Julie Marteau[c], Yves Berthier[a].

a Université de Lyon, INSA-Lyon, LaMCoS UMR5259, F-69621 France
b Université de Lyon, CNRS, INSA-Lyon, MATEIS UMR5510, F-69621 France
c Université de Technologie de Compiègne, Laboratoire Roberval de Mécanique FRE UTC-CNRS 2012, Centre de Recherche Royallieu, CS 60 319 - 60 203, Compiègne Cedex, France

Highlights

- Use of a new mechanical bench to reproduce realistic wheel-rail contact condition.
- Pure Mechanical White Etching Layer formation.
- Presentation of the microstructural response of the R260 steel as a function of the solicitation type (rolling, rolling with sliding).
- The efficiency of a tribological fuse layer that limits wear to enhance the formation of mechanical WEL is presented.

Abstract

This study presents a successful attempt to reproduce White Etching Layer (WEL) under pure mechanical conditions, with the use of a new experimental test bench with tests conditions representative of the wheel-rail contact. The effect of the presence of a run-in or corrosive fuse layer at the rail surface has a great effect on the microstructure evolution. This layer prevents wear and allows microstructural transformation of rail steel. First, a tribological analysis of the effect of the surface preparation on material flows in the contact, hardness evolution, and formation of WEL is presented. Then a multiscale characterization approach combining optical microscopy, scanning electron microscopy and near surface EBSD characterization at the sub-µm level has been carried out to understand the formation mechanism of such mechanically formed WEL.

The different scenarios of the wear behavior and microstructural transformation were drawn. The influence of the conditions of preparation of the sample surfaces, in particular of the presence of a tribological fuse layer (either a run-in layer or a corrosive layer) on the wear fatigue competition and the WEL formation, were also studied.

The normal stress due to the normal force in the tests leads to the formation of a hardened layer of nanograins. When submitted to shear in the rolling with sliding tests, this layer is removed by wear if the cohesion between the surface and the bulk is too weak. The presence of a fuse layer before the shear solicitation by sliding increases this cohesion, and turns the wear behavior into progressive microstructural transformation. Therefore White Etching Layer were formed through a mechanical process with realistic operating conditions avoiding the formation of thermal WEL.

© 2021 published by Elsevier. This manuscript is made available under the CC BY NC user license
https://creativecommons.org/licenses/by-nc/4.0/

1. Introduction

Railway transport is a very popular mean of transport due to its efficiency, its cost for the user and its lower impact on the environment with respect to road transports. The high frequentation of the railway networks causes a quick deterioration which is contained by maintenance operations. The Rolling Contact Fatigue (RCF) of rail steel, is one of the major concerns of railway networks for safety reasons. The accumulation of rolling and sliding loading at rail surface with wheel passes leads to the formation of defects that can cause the failure of the rail, as squats for instance. Their formation is usually associated to straight line tracks, and to acceleration and braking areas. Even if the dynamic response of the wheel rail contact and the development of squat defects has been widely studied [1]–[4], their initiation mechanism is not yet fully understood.

The White Etching Layer (WEL) and Brown Etching Layers (BEL) [5], which appear with white and brown contrast respectively after Nital etching on optical microscopy, are frequently found at squat surface at their early stage. For both phases, their high hardness with respect to the rail head leads to crack initiation at their interface with the bulk. The BEL consisting of “white and brown” sublayers, the present study will focus in the WEL formation[6]. Thus the investigation of WEL formation is one key toward the understanding of the squat birth.

The white etching layer is a Tribological Transformation of Surface (TTS) observed in steels. It is characterized by its high hardness (from 400 Hv up to 1200 Hv) [7], [8]. Two main types of WEL formed from two different mechanisms can be found.

One mechanism is associated to a thermal process, similar to martensite transformation during quenching [9]. The high pressure and shear stress at wheel-rail interface due to sliding and friction leads to flash temperatures reaching the austenitization threshold [8], [10], [11]. The latter can be lowered under hydrostatic pressure [12], [13]. The quick cooling leads to the formation of martensite, and sometimes residual austenite within the white etching layer [14]. Usually, a clear separation between the bulk and the thermally formed WEL is observed [15].

The other formation mechanism implies a mechanical process resulting in a high deformation of the steel. An accumulation of load combining pressure and shear stress can lead to the progressive deformation of the steel microstructure with a ratcheting phenomenon [16], [17]. In pearlitic rail steel, the cubic lattice of the ferrite deforms, allowing the migration of carbon atoms out of cementite [18]. An oversaturated and deformed ferrite is obtained: the white etching layer. This microstructure is similar to the one of martensite [19], [20]. The white etching layers obtained through a mechanical process show a progressive modification of the underneath layer below the WEL. The subsurface is highly deformed, presenting a reduction of inter-lamellae spacing, a reduction of the grain size and a progressive dissolution of the cementite [21].

It is also suggested that the two processes of formation can happen simultaneously and that one process can be predominant depending on the conditions [7], [20], [22]. In this way, white etching layers presenting simultaneously highly deformed ferrite, martensite, residual austenite, and fragments of cementite lamellae were observed [23].

In order to investigate their formation mechanism, WEL have been reproduced experimentally in laboratories. A part of the WEL described in the literature was formed with a thermal dominant process with respect to the mechanical one [24]. Some WEL were formed with a combination of a thermal and mechanical solicitations [13], [25]. Some other WEL were formed with a very high sliding condition up to -200% to -3000% of creep on twin-discs [24], [26] or wheel on rail test bench [27]

causing a high increase of temperature due to friction. These last conditions tends to form a WEL with a thermal dominant process which are not representative of the operating conditions on tracks. The vehicles in circulation are mostly equipped with anti-slip control, avoiding high sliding conditions even in acceleration and braking areas where some squats and white etching layer are observed (the slip threshold is lower than 2% in Paris Public Transportation) [20].

However, only few studies report WEL etching layer reproduced in laboratory with a dominant mechanical process, *i.e.* with test conditions representative of operating conditions. Indeed, these conditions should allow the application of a sufficiently high number of wheel passes with a significant but realistic sliding ratio, which is difficult to achieve. The conditions must be chosen in such a way to induce a progressive deformation of the steel microstructure with a ratcheting phenomenon, and to limit wear that may remove the white etching layer during its growth. For instance, it was observed on twin-discs machine under dry sliding conditions, that the accumulation of mechanical solicitations on a small area of contact due to disc dimensions can favor wear on the discs [28]. At the contrary, some strategies using the introduction of fuse layers to prevent wear under realistic rolling conditions on twin-discs were investigated, and brought encouraging results [29]. These conditions were used in the present study.

This study presents the experimental reproduction of WEL mechanically formed, with the use of a new experimental test bench with representative tests conditions. The effect of the presence of a fuse layer on the surface on wear is then studied. Two strategies were adopted to create the fuse layer: the first consists in creating a mechanical hardened surface by pre-rolling with pure normal conditions; the second consists in the formation of layer of corrosion at the sample's surface before the tests. First, a tribological analysis of the effect of the surface preparation on material flows, hardness, and formation of WEL will be presented. Then a multi scale characterization approach combining optical microscopy, scanning electron microscopy and near surface EBSD characterization at the sub-µm level has been carried out to understand the formation mechanism of such mechanically formed white etching layers.

2. Method and material

In order to reproduce the rolling contact conditions, a novel test bench was developed called Triboring, Figure 1. It consists in a small disc of diameter 70mm (representing the wheel), rotating on a horizontal circular ring of diameter 2 m (the rail).

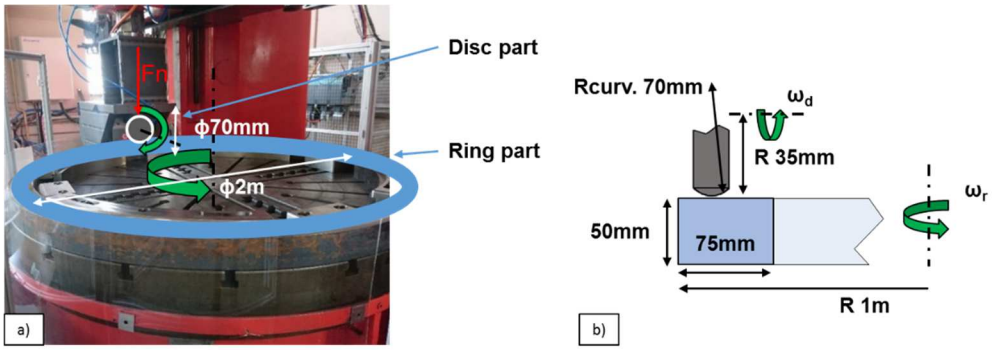

Figure 1 Triboring test bench, a disc in rotation on a circular rail (the ring)

The rail part is made of a 2 m diameter forged ring of R260 steel bloom with a rectangular section 75 mm x 50 mm, which in similar to the rail head dimensions. The microstructure and composition of the alloy can be found in [30]. The thermal process applied during the ring-rolling forging is the same as the one applied on R260 rails. The microstructure obtained is then similar to the one observed in new rail (similar hardness, phases and grain size), with a fully pearlitic microstructure [31]. The ring surface is machined in order to remove the calamine layer.

The wheel part is a convex disc from R260 head rail (Ra 0.8 µm). Its rotational speed is directly linked to the measured rotational speed of the ring. Taking into account the radius of the disc and its position with respect to the center of the ring, a factor between the rotational speed of the disc and the ring is defined to apply a sliding ratio at the contact. A static vertical load is applied on the disc in order to obtain the desired theoretical pressure at the contact. Several parallel tracks can be realized on one disc, by changing the radial position of the disc of a few centimeters, with respect to the center of the ring part. Therefore, several tests are performed on each ring.

Two "standard" test conditions close to the operating conditions were defined for each ring tested: a pure rolling test (for cruising speed areas) and rolling with sliding conditions of 0.5% (for acceleration and baking areas). The sliding ratio was calculated using:

$$\gamma = \frac{V_d - V_r}{V_d + V_r} = \frac{R_d\omega_d - R_r\omega_r}{R_d\omega_d + R_r\omega_r}$$

With V_d and V_r the speed of the disc and the ring at the point of contact, ω_d and ω_r their rotational speed, and R_d the radius of the disc and R_r the minimum distance between the center of contact and the center of the ring.

This sliding ratio of 0.5% is relatively low compared to the experimental tests leading to WEL formation observed in the literature (10% in [26], >100% in [24] and-300% to -3000% of creepage in [27]). The goal is to have a realistic sliding ratio (<2%) and to avoid the formation of thermal WEL. This sliding ratio was fixed to be sufficient to initiate mechanical WEL formation in [29]. With those conditions of contact (radii of curvature, material properties and normal force applied), the theoretical Hertz contact dimensions are 0.55 mm and 0.86 mm (half-width). For all tests, the ring

rotation speed is set to 21.6 rpm, the theoretical Hertzian pressure is 1 GPa, (equivalent to a normal force of 1 kN in the present configuration). The common data of the test conditions are summarized in Table 1

Standard test conditions	
Ring steel	R260
Disc steel	R260
Disc Radius	35 mm
Disc Radius of curvature	70 mm
Ring linear speed	2.26 $m.s^{-1}$
Theoritical Hertzian pressure	1 GPa
Normal force	1 kN

Table 1: Summary of the common test conditions

The experiments of this study are divided into three test series corresponding to three rings (ring A, B and C) which are summarized in Table 2. Those three test series were performed with three different surface treatments: extensive surface cleaning with ethyl acetate of the discs (tests on Ring A), regular surface cleaning of the discs (tests on Ring B), and surface corrosion of the discs and the ring (tests on Ring C).

The extensive cleaning correspond to a cleaning of the discs with ethyl acetate, then ultrasonic bath with ethanol for 5 minutes. The regular cleaning is simply the ultrasonic bath with ethanol for 5 minutes. For the “surface corrosion” treatment, the discs are submitted to a regular cleaning, and then left in water in a container for 24h in a ventilated room (causing the complete evaporation of water). The ring surface is also submitted to corrosion: a thin film of water is poured at the ring surface and left for 24h. After complete water evaporation a powdery layer of natural corrosion is formed. In order to obtain a homogenous and more cohesive layer, the operation is repeated three times.

Series (surface treatment)	Test #1 Pure Rolling	Test #2 Rolling with sliding	Test #3
RING A Extensive cleaning	1,000 cycles 0% sliding	1,000 cycles 0.5% sliding	none
RING B Regular cleaning			1,000 cycles, 0% + 1,000 cycles, 0.5%
RING C Corrosion on surface			3,000 cycles, 0.5%

Table 2: Summary of the mechanical tests performed

Each test (#1, #2 and #3) corresponds to a track on the same ring. A tribological analysis of the tracks surface is performed after observation with an optical microscope. The material flows are studied mainly qualitatively with the third body concept (See ANNEX: Conceptual tools: Third body and flows), which was already used for previous wheel-rail contact analysis [32], [33].

For every test in rolling with sliding condition (RING A, B, C Tests #2 and #3),it can be noticed that the ratio between the longitudinal force measured and the normal force were similar, close to 0.3.

For every rings, after each set of tests, the ring is carefully cut with no temperature increase up to 50°C to extract track samples. The tracks cuts are observed with an optical microscope after mechanical polishing and Nital etching. The sample were also prepared for observations in Secondary Electron (SE) mode in the Scanning Electron Microscope (SEM) and for Electron BackScatter Diffusion (EBSD) mode. For the SE mode, the sample were etched with Nital, for a better observation of the cementite lamellae and to reveal the possible WEL. For the EBSD mode, the sample were mechanically polished up to 1 µm. For some cross section samples, it was possible to carry out an additional ionic polishing with a PIPS ILLION 2 with accelerating voltage 4 kV to obtain a clean sample surface state very close to the surface edge. The observations were performed with different microscopes: a FEG Zeiss Supra 55VP equipped with an Oxford EBSD Symmetry detector with an accelerating voltage set to 12 to 15 kV, a FEI Quanta 600 with an accelerating voltage of 20 kV, and a FEG Zeiss Σigma 600 with an accelerating voltage of 25 kV. The EBSD data treatment was realized using Atex software [34].

3. Results

3.1. Mechanical conditions to reproduce WEL: effect of the fuse layer on wear and WEL formation.

3.1.1. Ring test with extensive cleaning of the discs (ethyl acetate): Ring A

For both samples (Test #1 and Test #2), the optical microscopy observations of the surface revealed an important enlargement of the track width compared to the track width after the first wheel turns. The latter was close to theoretical hertz calculation of contact patch width. The limits of the track width can be identified from the machining marks of the rail, which are visible on the two external parts of the track. On the pure rolling test (Figure 2a), the track width is about 6.1 mm (+/- 0.2 mm). Along the track width, only one major strip can be observed. This strip presents a longitudinal flow of 3rd body (Q_iLon-3rd) (See ANNEX: Conceptual tools: Third body and flows and Figure 20). The irregular profile of this layer presents higher peaks than the machining marks. This highly suggests that it corresponds to a spread of particles coming mainly from the disc rather than particles from the disc itself. For the 0.5% sliding test, (Figure 2b), the tracks width is about 6.8 mm. One central strip (I) shows a rather smooth and homogenous aspect. The profile on this part is slightly lower than the machining marks, highlighting the wear of particles from the ring. On the two outer strips, the profile and the black particles shows the accumulations of 3rd body particles on the side of the contact, which correspond to a lateral flow (Q_iLat-3rd).

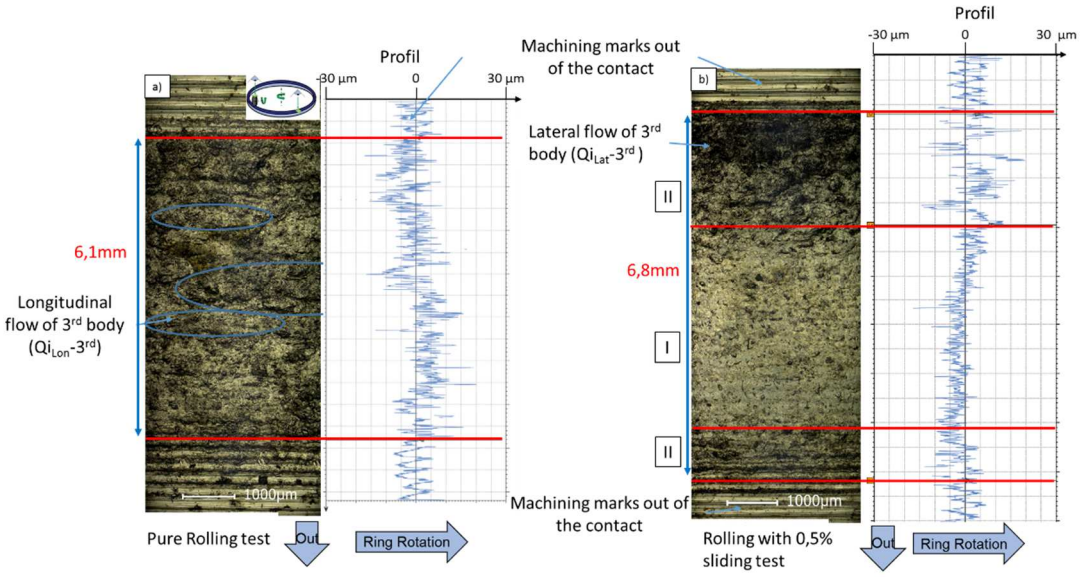

Figure 2 Surface observation and profile measurement of the ring A, observed with optical microscope for a) pure rolling test (test #1) – track width=6,1mm and b) rolling with sliding test (test #2) – track width=6,8mm. The track border is indicated as a red line

The different aspects of the two tracks can be explained with the following elements:

The disc rotates about 28 more times than the ring, therefore a predominant detachment of particles can be expected from the disc part.

In pure rolling test, the detachment of particles from the two bodies should be lower than in presence of sliding. The absence of sliding in the contact is suitable to accumulate the 3rd body particles detaching from the disc.

In rolling with sliding conditions, the 3rd body particles within the contact tends to be ejected, and some detachment of particles from the ring can be observed even for a low number of cycles.

This behavior is confirmed by scanning electron microscope observations in SE mode. The Figure 3 shows a longitudinal section of the ring in the middle of the track, for the pure rolling test (a) and for the rolling with sliding test (b). On the pure rolling test, the detachment of 3rd body particles appears as a thin strip of 5 to 10 µm thickness. On the rolling with sliding test, the same phenomenon is observed, as well as a thicker band of 10 to 20 µm of mater from both 3rd in surface and 1st body from the ring (Source flow Qs).

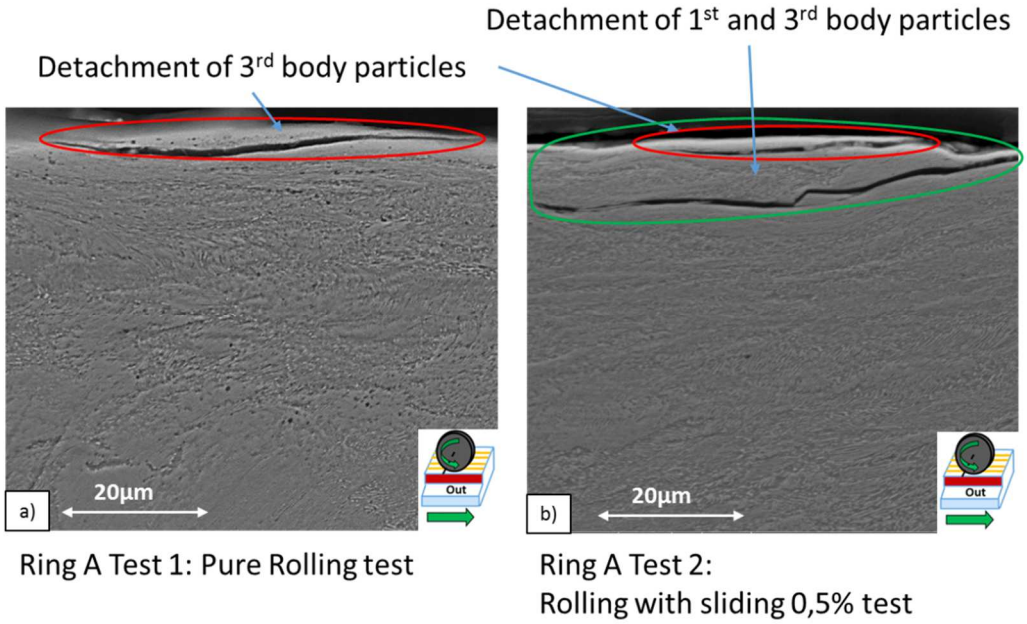

Figure 3 Longitudinal cut of the ring part, observed with scanning electron microscope for a) test #1 pure rolling test and b) test #2 rolling with sliding test

These observations after 1,000 ring rotations show a massive flow and detachment of 1st and 3rd body particles which is not representative of the real wheel-rail contact. This is similar to the considerable wear observed during the twin disc test in absence of fuse layer[29]. Regarding the flow description of the Figure 2, this means that the source flow Qs-disc from the disc first body is too massive in the pure rolling test. In the rolling with sliding test, the source from the two first bodies (Qs-disc and Qs-ring), and the wear flow Qw are too important to be representative of the real conditions. This can be explained by the stronger adhesion of the disc and ring surfaces compared to the cohesion of the disc material itself. The high adhesion is possible because of the important pre-cleaning of the surfaces and the probable activation of the dangling bonds as developed in [29]. As a consequence, another series of tests were performed with a limited cleaning of the surface to limit surface adhesion and therefore wear.

3.1.2. Ring test with regular cleaning of the discs (without ethyl acetate): Ring B

The cleaning process was modified (regular cleaning) to avoid an excessive adhesion of the surfaces in contact due to the extensive cleaning with ethyl acetate. After standard pure rolling test condition (test #1), the track width was almost divided by 2 with about 3.5mm width against about 6.1mm previously on ring A (Figure 4(a) and Figure 2(a)). In the middle of the track, some evidence of a limited longitudinal flow of 3rd body Qi_{Lon}-3rd is visible. The contribution of 3rd body creation by detachment of particles from the disc is thus lower than previously (low Qs-disc and Qw). Some marks of machining can also be observed, indicating the relatively low wear rate of the ring (low Qs-ring and Qw). The resolution of the profile measurements of the following tracks was not sufficient to bring a reliable quantitative value of the wear rate. The second track corresponds to the standard rolling with sliding test Figure 4b). The surface of the ring presents a different aspect from the previous pure rolling test. The track width is enlarged to about 4.1mm against about 3.5mm. Almost no evidence of 3rd body flow coming from the disc or machining marks are visible on the track surface. This indicates a probable detachment of particles from the ring (Qs-ring), and the ejection of the 3rd body particles (Qw) from the contact.

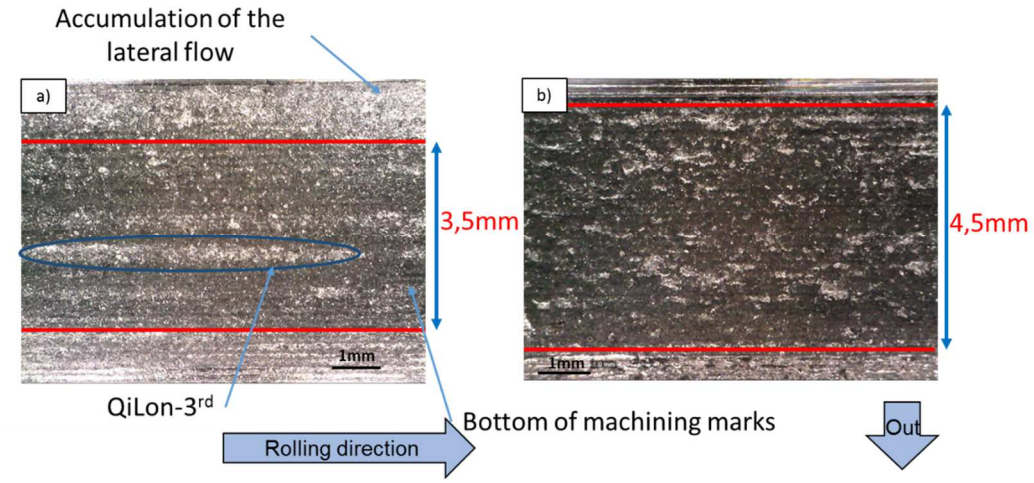

Figure 4 Surface observation with optical microscope on ring B of: a) the pure rolling test (test #1) on ring B, b) the rolling with sliding track (test #2). The enlargement of the track width is clearly visible.

This is confirmed by the SEM observation of the longitudinal cut in SE mode. The Figure 5 presents the two typical morphologies of the track surface after the rolling with sliding test. The Figure 5a) presents the deformation of the surface due to shear stress induced by sliding. The Figure 5b) exposes detachment of a thin lamellae of the steel ring. Such observations, representative of whole surface of the rolling with sliding test, were barely observed on pure rolling test tracks.

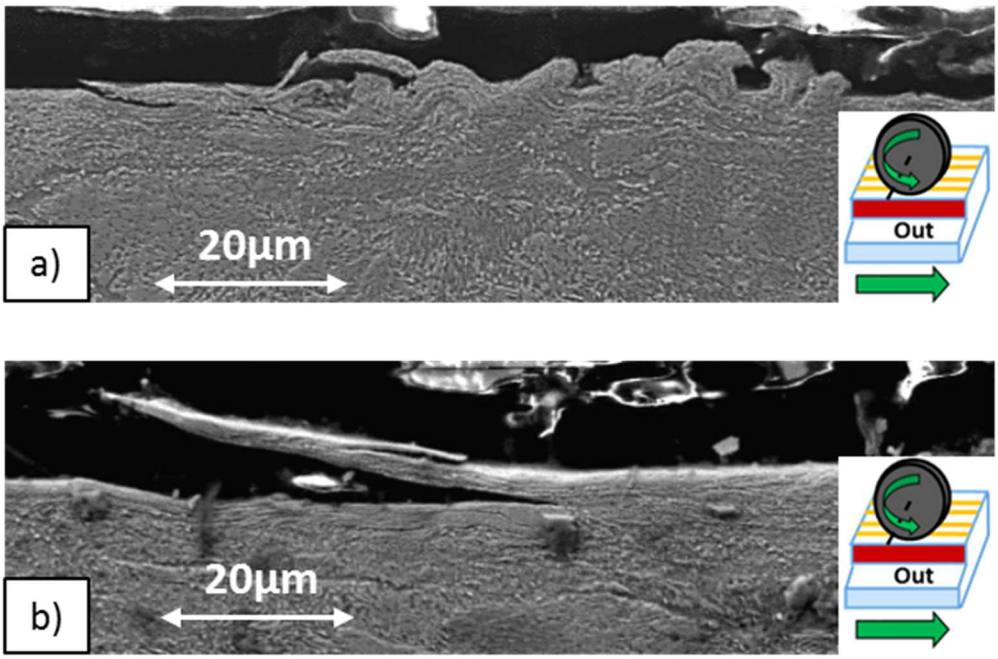

Figure 5 Longitudinal observation with scanning electron microscope (SE mode) of the ring subsurface showing the effect of shearing due to sliding in Ring B test #2: a) deformation of the surface, b) detachment of particles

The test with sliding analysis proves that the detachment of particles and wear is too important on the ring part, which is consistent with the field observations. It does not enable to reach a possible transformation of the pearlite at the surface into white etching layer, despite the improvement of wear rate with the change of cleaning protocol.

In order to prevent such early particles detachment, the third test condition was run to assess the influence of a tribological fuse. This tribological fuse is made of a run-in layer at the ring surface, created during 1,000 cycles of pure rolling. After this pre-test the disc is changed for a new one for the standard rolling with sliding test. Therefore, the surface microstructure of the ring before the rolling with sliding test is no more undeformed pearlite but the deformed state reached at the end of the standard pure rolling test. The track of sliding test with a run-in fuse layer in Figure 6 shows two distinct parts. The middle one with 3.5mm width, which was the width of pure rolling test track. No machining marks or evidence of noticeable 3rd body can be seen. On the other hand, the two boundaries present an accumulation of 3rd body particles on 0.5mm width. Considering the fact the track is not larger than the one of the previous tests, and that this tracks went through to 2,000 cycles (1,000 for the run-in and 1,000 for the sliding) against 1,000 for the two previous tests, the wear is less important than the standard rolling with sliding test without fuse layer. This qualitative observation highlights the importance of a tribological fuse layer on the switch between wear and fatigue mechanisms.

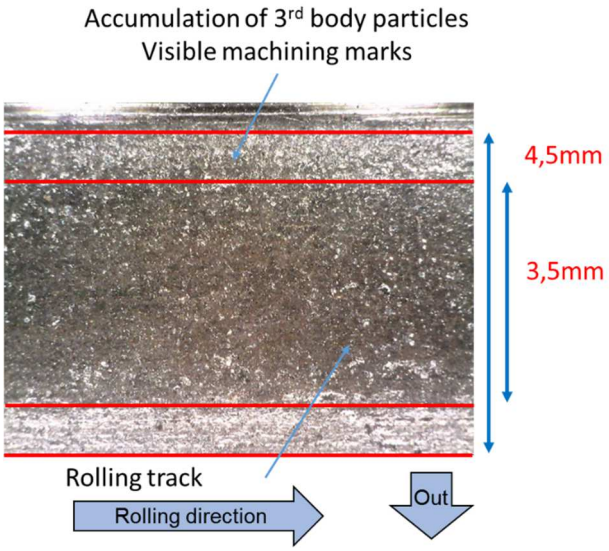

Figure 6 Top view of the rolling with sliding test track on rail B after the creation of the fuse layer by 1000 cycles of pure rolling (test #3).

For each tests, $HV_{0.1}$ hardness measurements were performed three times every 70 µm from 20 µm (in order to avoid edge effect at the surface) to 1350 µm of depth. Additional measurements were made out of the track. The results, Figure 7, reveal that the hardening is globally more important after pure rolling test (red line) than after sliding tests. A hardness of 350 HV (+/-5) is measured at 20 µm for the pure rolling tests, whereas it is 325 HV (+/-12) for the pure sliding condition, and 335 HV (+/-15) in the case of the test with fuse layer. A decrease in hardness with a similar slope is observed for the three sample. At 250 µm depth the same hardness is observed in the track as in the reference material.

The same pure normal force is applied for all tests, which should lead to a similar surface hardening. However, the surface observations indicated that sliding conditions lead to more wear, which can be the cause for the apparent shift of the curves towards higher depth. One can see that, in the case of the fuse layer, the surface hardness is slightly higher than the one of the pure sliding test. This demonstrate the beneficial aspect of the creation of the fuse layer for the limitation of wear. However, the hardness level observed in surface for this sample are far from the ones expected in the case of a WEL.

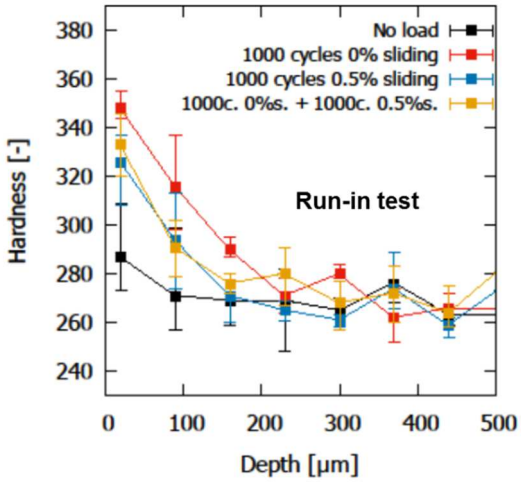

Figure 7 Hardness measurements along depth for each test track on rail B: Black: out of track, Red: standard pure rolling (test #1). Blue: standard rolling with sliding (test #2). Orange: rolling with sliding after fuse layer formation (test #3).

Nevertheless, even with a run-in fuse layer, the detachment of particles is still too important which shows that this layer is not sufficient to reproduce the wheel-rail contact reality, and has to be improved. The previous study [29] showed better results in WEL initiation on twin disc tests with the presence of a corrosion layer at initial state.

3.1.3. Ring test with corrosion fuse layer on ring and discs surface: Ring C

A layer of corrosion was created at the ring and discs surface as described previously. Based on field observation of the real wheel-rail contact environment, it looks natural to add a corrosion layer on top of the rail prior any test.

The same tests as for the Rail A and B were performed (Test #1 and #2). It's been possible to extend the sliding test up to after 3000 cycles thanks to the presence this corrosion fuse layer, which is expected to prevent massive wear of the track (Test #3).

3.1.3.1. Track surface observation

The comparison in the Figure 8 of the top views of the pure rolling test track and the rolling with sliding test track, shows several similarities. The two tracks have the same width (7 mm), which indicates a similar wear level (Qw) even with different sliding conditions, and both present five strips. The profile of the tracks could not be provided due to the important light contrast between the orange corrosive fuse layer and the shiny track. The use of a mechanical profilometer would have damaged the track surface. On the areas 1 and 2, the corrosive fuse layer was fully removed. On area 1 in the middle of the track, the surface is rather shiny and presents very few 3rd body flow in the longitudinal direction. On areas 2, the amount of 3rd body flow is more important (Qi 3rd). These transition strips correspond to the progressive accumulation of 3rd body due to the progressive enlargement of the width of contact from the center to the borders. On the sides, the strips 3 correspond to the areas were the discs made a lower amount of cycles. Thus, the corrosive fuse layer is not fully detached and the machining marks can be spotted. These observations indicate a relatively low amount of wear.

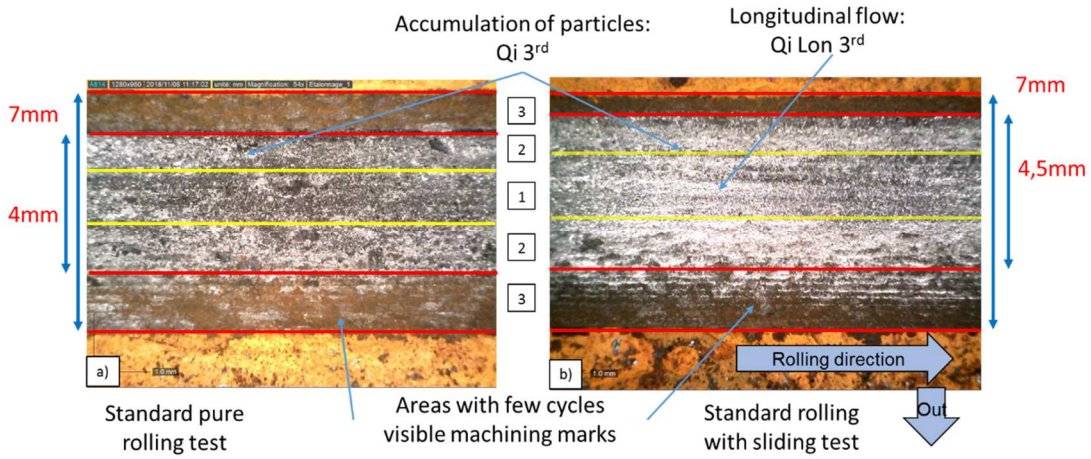

Figure 8 Ring C, Top view of: a) the standard pure rolling test track (test #1), b) the standard rolling with sliding test track (test #2)

After the fuse layer formation and 3,000 cycles rolling with sliding test (test #3), on Figure 9 the width of the track is similar to the two previous tests, but the accumulation of 3rd body, and the width of the strips 2 are more important. This indicated that the detachment of particles from the ring part is probably similar to the previous test #2 on ring C (Figure 8b)) with a corrosive fuse layer (Qs-rail), but the detachment of particles from the discs is more significant (Qs-disc).

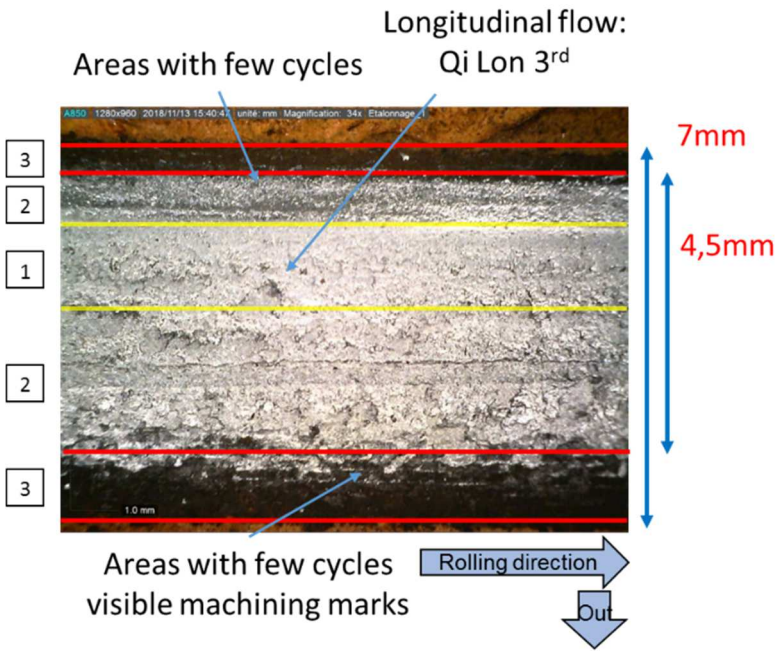

Figure 9 Ring C Top view of the 3,000 cycles rolling with sliding test track (test #3)

The hypothesis is reinforced by the hardness measurement on Figure 10 at 20 µm depth. After pure rolling (test #1) and after pure sliding without fuse layer formation (test #2), similar mean hardness at 20 µm. The pure rolling test (test #1) presents a slightly higher hardness (310 HV) than the one for the rolling with sliding test (test #2) (295 HV).

3.1.3.2. Hardness results

With the creation of the corrosion fuse layer, a significant increase in hardness is observed at the end of the tests, even in rolling with sliding test with 370 HV measured at 20 µm depth for 3000 cycles. This is much more than what was observed in the case of only 1,000 cycles with 295 HV. This indicates that the hardening of the steel seems faster that the detachment of ring particles at the surface. Therefore, this means these operating conditions are favorable to the steel microstructure transformation and then, to the mechanical formation of the WEL, with regard to wear/fatigue competition.

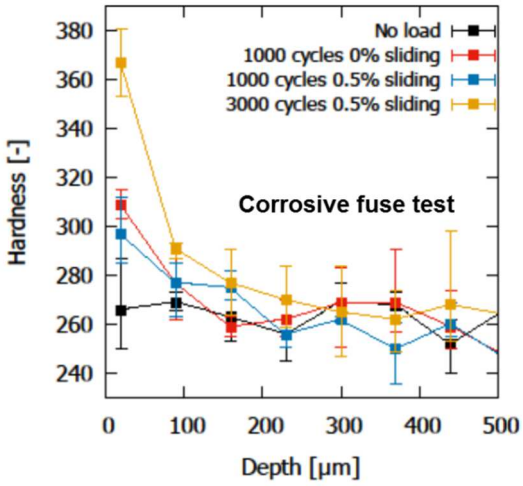

Figure 10 Hardness measurements along depth for each track of the corrosive fuse layer tests (Ring C). Black: out of track, Red: standard pure rolling test (test #1). Blue: standard rolling with sliding test (test #2). Orange: 3,000 cycles standard rolling with sliding test (test #3).

3.1.3.3. Cross-section SEM analysis

Some longitudinal cut have been etched with Nital in order to evaluate the presence of WEL. The Figure 11 show observations with scanning electron microscopes of the 1,000 cycles rolling with sliding test. A singular bright layer of 5 µm at the surface is observed at different localization along the sample. The frontier with the subsurface is locally uncertain and progressive. On the sample corresponding the longitudinal cut of the 3,000 cycles rolling with sliding test, the layer observed is thicker (5-15 µm). The spots observed along the surface are from 10 to 100 µm long. The layer is darker but its aspect is quite homogenous with no evidence of lamellar microstructure.

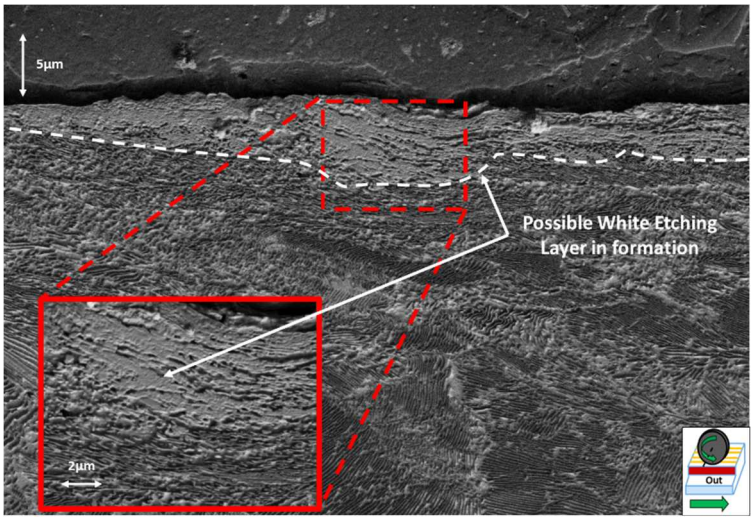

Figure 11 Longitudinal cut of the rail track of the standard rolling with sliding test after Nital etching (Ring C, test #2) a) observation with optical microscope, b) observation with scanning electron microscope (SE mode) – the presence of a WEL is clearly visible at the ring surface

The Table 3 summarize the main trend of the tests performed on the wear observed and the formation of WEL. The effects of the mechanical loadings and the presence of fuse layer on the microstructure will be described and analyzed in the following part.

Details of test conditions in Table 1 and Table 2	Test 1 1,000 cycles Pure Rolling	Test 2 1,000 cycles Rolling with sliding	Test 3 B: Rolling then sliding C: 3,000 cycles Sliding
RING A Extensive cleaning	Wear: important no WEL	Wear: important no WEL	none
RING B Regular cleaning	Wear: significant no WEL	Wear: important no WEL	Wear: few no WEL
RING C Corrosion on surface	Wear: few no WEL	Wear: few **Probable WEL**	Wear: few **Probable WEL**

Table 3 Summary of mechanical tests types on Wear and WEL formation

3.2. Microstructural transformation due to mechanical solicitations

3.2.1. Observation on Ring B

In order to better understand the microstructural mechanism leading to the formation of the run-in fuse layer and the mechanisms leading to the apparition of WEL, the microstructure of selected samples was characterized using EBSD.

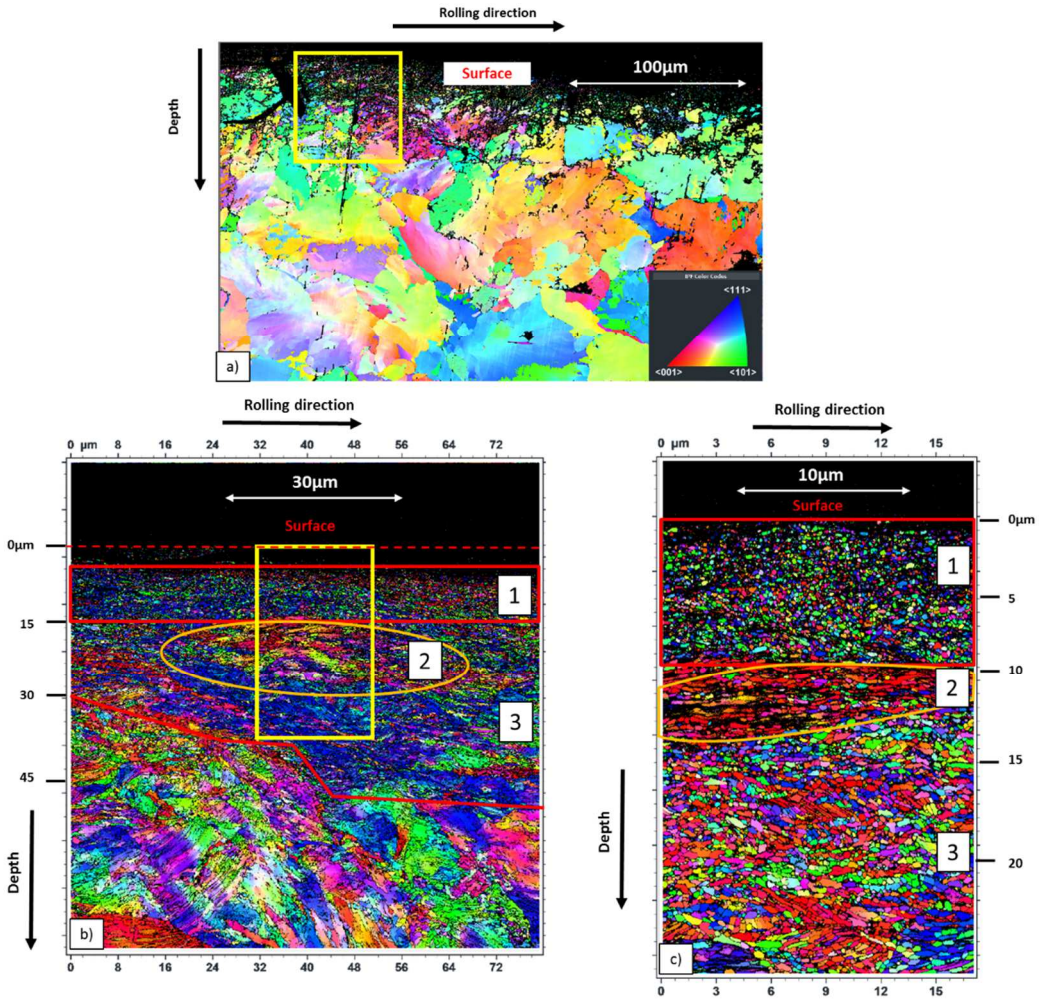

Figure 12 : (a-c) IPF X maps of a longitudinal cut of the ring B sample for the pure rolling test (test #1). The yellow rectangles in (a) and (b) are indication of localization of the maps (b) and (c) respectively. Depending on the depth, three microstructures noted (1),(2) and (3) are visible, and are separated by red lines.

The microstructure of the pearlitic steel before deformation is observed on the bottom of Figure 12a). It consists of pearlite nodules of around 60 µm in diameter, with a relatively uniform crystallographic orientation in each nodule. The cementite layers are not visible at this scale. After the standard pure rolling test, the microstructure is affected by the deformation on the first 60 µm. As the deformation tends to break the nodules and increase the dislocation density, smaller nodules are visible close to the surface, and the indexation rate drops so that the microstructure is barely visible on the last 50 µm. When adding an ion polishing step for the material preparation, and decreasing the step size as well as the accelerating voltage, the indexation rate can be significantly improved so that the microstructure can be observed up to the first micrometers beneath the surface (Figure 12b) and c)).

A gradient of microstructure as a function of the depth is clearly visible on Figure 12b). Three different zones where different microstructures are identified. The zones are separated by red lines on Figure 12b) and c), and denoted (1), (2) and (3).

For depth between 30 to 60 µm (zone 3), the nodules of pearlite are deformed so that their identification from their orientation color becomes difficult. Some pearlite colonies remain recognizable from the ferrite and cementite lamellas that are not fragmented. For similar depth, one can see that some areas are more morphologically deformed than others, which implies that the

local deformation is dependent on the orientation of the colony, with respect to the deformation stress induced during the test.

For depth from 8 µm to 30 µm, a second microstructure was identified as (2). Note that the transition between zone 2 and zone 3 is not clear, as the microstructural changes are not abrupt but follow a gradient. In this area, where the morphological deformation is much higher than in zone (3), the nodules cannot be identified any more, and the pearlite colonies are fragmented. Moreover, the fragmented entities tend to align parallel to each other and to the surface, in the direction of stress. This is particularly visible in the area encircled in orange, where all fragments present a similar orientation and are well aligned parallel to the surface. Therefore, the realignment of the fragmented part is dependent on the original orientation of the pearlite with respect to the macroscopic stress. The fragmented parts present a length of around 1 µm and a thickness of around 0.5 µm. This type of fragmentation and realignment of the lamellas was already observed during high deformation of R260 steel [30], [35]–[37]. In [38] a similar microstructure was investigated by transmission electron microscopy (TEM), and revealed that, even if the lamellas are reduced and are realigned, cementite layers are still present between the lamellas.

Finally, for depth between the surface and 8 µm, the intense deformation gave rise to a population of spherical grains few hundred nm in diameter (zone 1). The microstructure of the pearlite has completely vanished and no nodules or lamellas can be identified anymore. The interface between zone (1) and zone (2) is much sharper than the one observed between zones (2) and (3).

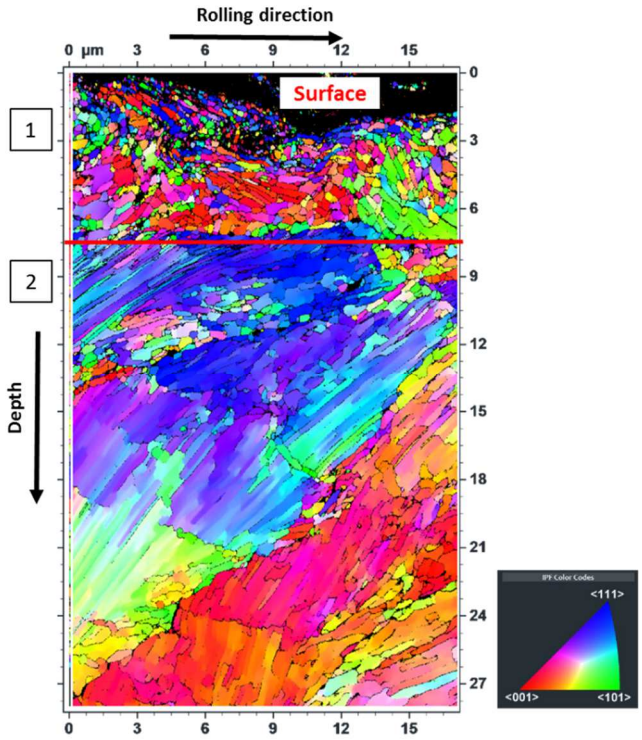

Figure 13 : IPF X map of a longitudinal cut of the ring B sample after rolling with sliding test (test #2), indexation step 0.07 µm

The microstructure observed after sliding tests is presented on Figure 13. From the surface to the red line (about 10 µm depth), the microstructure is made of pearlite nodules partially fragmented, similar to zone (2) presented in Figure 12. It is composed of slender entities (1 to 1.5 µm long) with the same crystallographic orientation. The layer (1) observed in the case of pure rolling, consisting of circular entities of diameter (0.1-0.5 µm) is not present in this sample. Deeper, the microstructure is

quite different: the nodule of pearlite are elongated along the sliding direction because of the shear stress induced. Furthermore, a strong disorientation is observed within the nodule, characteristic for plastic deformation. Such deformations are not visible any more for areas deeper than 30 µm.

On the test #3 of ring B after the formation of a run-in fuse layer, the three areas found in the pure normal test sample are also observed: (1) first 7-8 µm consisting of 0.1-0.5 µm diameter spherical entities, (2) to about 15 µm depth with slender entities of 0.5 to 1 µm long, and (3) to 30 µm with partially fragmented pearlite nodules. For depth greater than 30 µm, a similar microstructure as the one of the undeformed steel was observed.

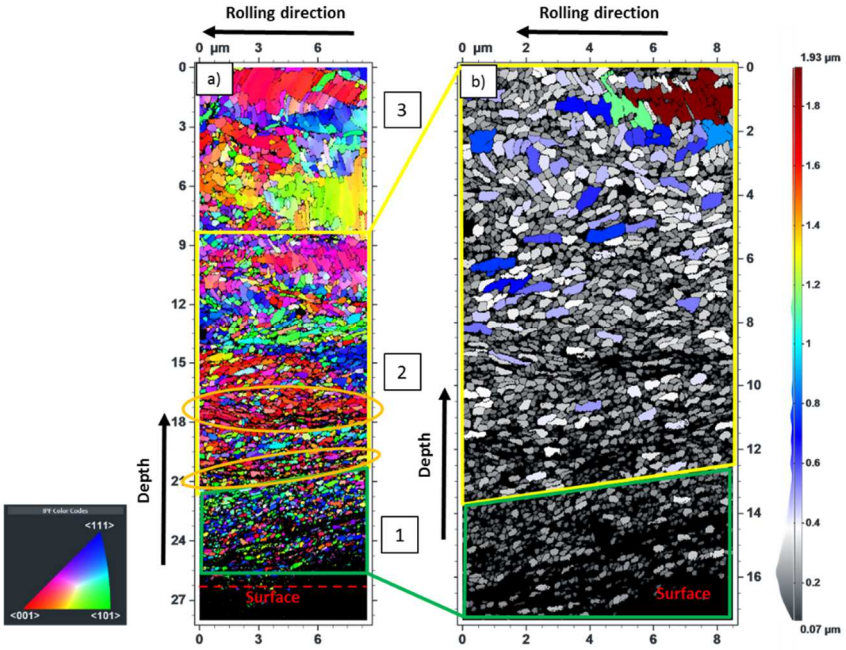

Figure 14 EBSD maps of longitudinal cut of rail samples on ring B after fuse layer formation (pure rolling + rolling with sliding test: test #3): a) IPF X map b) grain size map, zoom of areas 1 and 2 on map a), indexation step 0.02 µm

The hardness measurements at the surface or close to the surface of Figure 7 can be correlated to the microstructural state. The high level of hardness corresponds to the most important refinement of the pearlite into small circular entities. It is observed for limited amount of wear and thus to the part of material which was solicited by rolling with no or few particle detachment. The energy was mainly dissipated into the modification of the microstructure and first body flow (Qi-rail) for the test pure rolling test and rolling with sliding test with a run-in fuse layer. Whereas the energy was also dissipated into detachment of particles (Qs-rail Qw) for the rolling with sliding test.)

3.2.2. Effect of oxidation on the fuse layer (Ring C)

The EBSD maps of the Ring C could not be prepared with the same protocol used for the previous test series due to technical reasons. Therefore, it was not possible to obtain a sufficient indexation ratio to observe properly the layer very close to the surface (from 0 to 20 µm), and some uncertainties remain concerning the exact state of the microstructure. Nevertheless the sufficient quality of the map and the scenarios proposed for the previous tests, enable to suggest a microstructure transformation scenario for the corrosive fuse layer test series of Ring C.

The Figure 15 compare the IPF maps of longitudinal cuts of the pure rolling test (a) and the rolling with sliding test (b). The yellow rectangles marks out the approximate limit between the area close to the surface where the pearlite nodules seem to be rather fragmented, and a deeper area were the pearlite nodules are not fragmented. On the pure rolling test, this depth is close to 25 µm while it is lower than 20 µm for the rolling with sliding test. The slight different of thickness of this subsurface layer is consistent with the slight difference of hardness and particles detachment (Figure 8 and Figure 10). On the rolling with sliding test, the red curves from 20 to 40 µm highlight a morphological deformation of the pearlite nodules in the sliding direction. Such deformation is not observed on the pure rolling test. Considering these observations, it is suggested that the microstructure of the pure rolling test with a corrosive fuse layer (Ring C test 1) is similar to the one of pure rolling test of Figure 12 (Ring B test 1). Similarly, the microstructure of the rolling with sliding test with a corrosive fuse layer (Ring C test 2) is close to the one of a rolling with sliding test with a run-in fuse layer on Figure 14 (Ring B test 2).

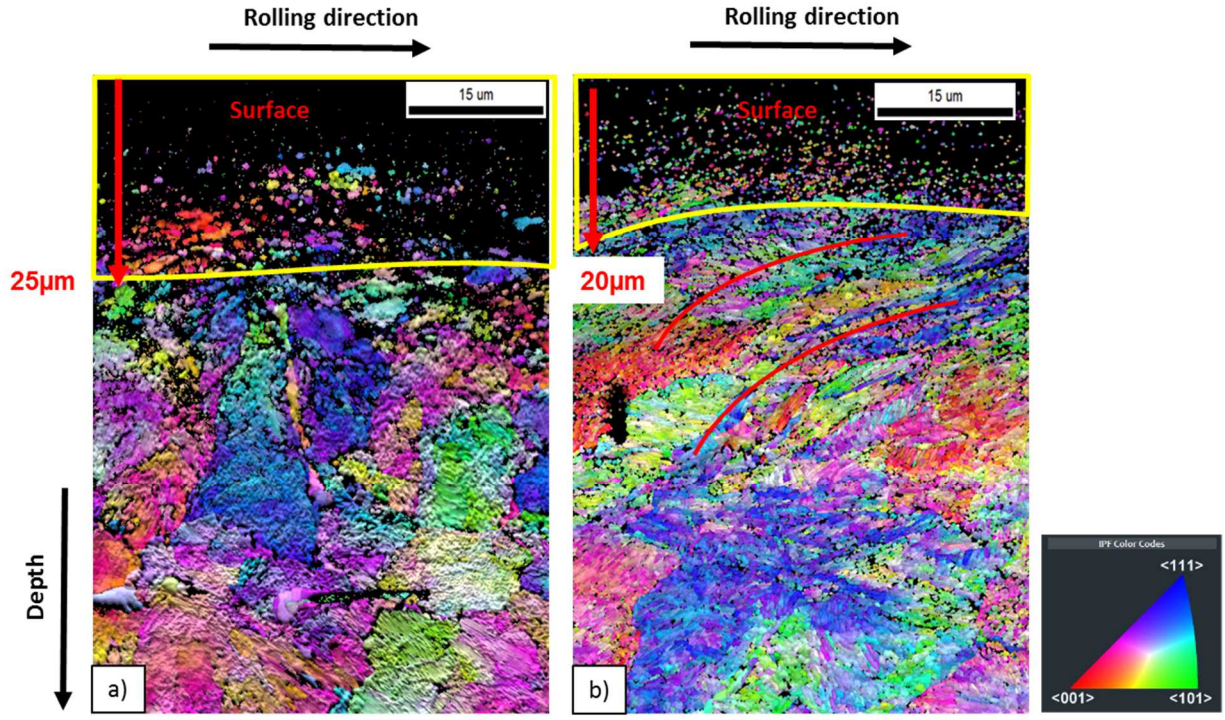

Figure 15 EBSD maps on ring C combining IPF map and Band Contrast of longitudinal cut of ring sample for: a) standard pure rolling test (test #1), b) standard rolling with sliding test (test #2), indexation step 0.1 µm

The Figure 16 is an IPF map of a longitudinal cut of the 3,000 cycles rolling with sliding test. The global aspect of the IPF maps of these two sliding tests (Figure 15b) and Figure 16) is similar with a scale difference. They both presents pearlite nodules close to the surface which are both morphologically deformed in the sliding direction and fragmented. This layer of fragmented pearlite nodule seems to be much larger for the 3,000 cycles test (about 40 µm) than for the 1,000 cycles test (about 20 µm). This enlargement of the fragmented nodules layer and the hardening of the surface and subsurface is consistent with a microstructural transformation rather than a particle detachment. WEL was observed in that last sample Figure 11, meaning that such microstructure favors the formation of mechanical white etching layer.

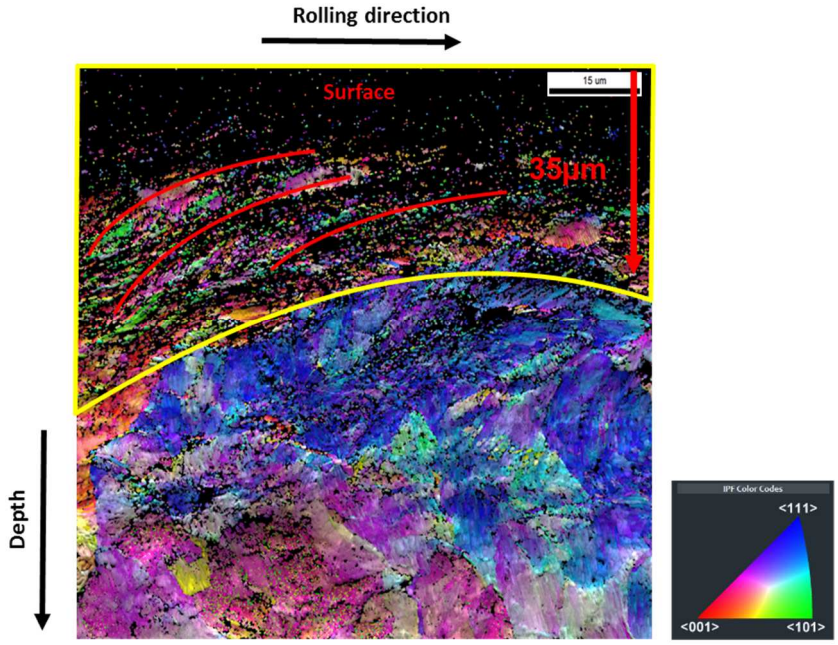

Figure 16 EBSD maps on ring C combining IPF map and Band Contrast of longitudinal cut of ring sample for the 3,000 cycles rolling with sliding test (test #3), indexation step 0.1 µm

4. Discussion

The three different types of microstructural organizations observed on different cross-sections of Ring B are sketched on Figure 17. They are placed side-by-side with a vertical shift corresponding to an estimated initial surface. Thus, the relative positions of the sketches illustrate the depth of wear.
The samples (corresponding to tracks) were submitted to different types of solicitations. A normal stress for every tests due to the normal force applied on the contact, and a tangential shear stress in the specific case of rolling with sliding. Depending on the solicitation and the presence of a fuse layer, the microstructure responses were different.
The normal stress induced a refinement of the microstructure with the observation of two levels of fragmentation in the subsurface (Figure 17 (a) and (c)): circular nanograins (0.1-0.5 µm) in the first micrometers below the surface, and circular nanograins with slender entities (1-1.5 µm) which must be lamellae fragments. The frontier with the deeper phase presenting unfragmented nodules is sharp. In case of shear caused by sliding, the microstructure has two mains responses between the surface layer and the deeper layer of material, which can be the signature of the cohesion of these layers:

- In some case (weak cohesion), the surface layer tends to detach from the sample, leading to wear (Figure 5b) and the removal of the layer of nanograins (Figure 13 and Figure 17). This could be the sign of a weak cohesion of the surfacic layer
- In some other case (stronger cohesion, the material tends to deform. It can be surface deformation as presented in Figure 5a), which tends to detach later on, or deformation of the microstructure which tends to keep deforming deeper under the surface. The nodules of pearlite can present a crystallographic reorientation, or/and a morphological deformation. The results of the run-in fuse layer sample (Ring B test 3) indicates the crystallographic reorientation of the nodules happens

before the morphological deformation. This was already observed in the same rail steel in the study of Head Check development by Dylewski on rails on field [39]. In this case, we can

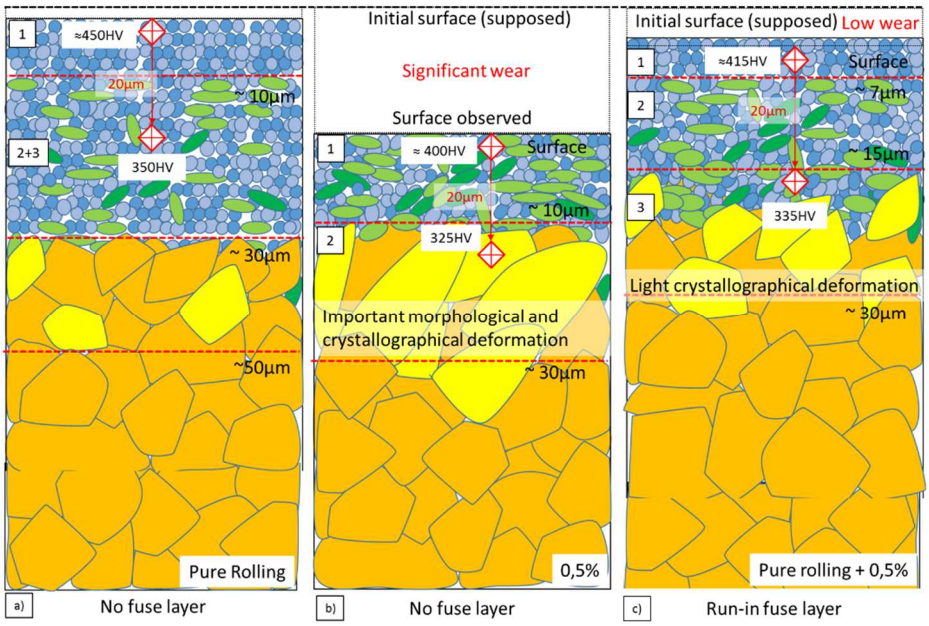

Figure 17 Schematic representation of the microstructure of the tests of Ring B (a) test #1 – no fuse layer, pure rolling (b) test #2 – no fuse layer, sliding (c) test #3 – Run-in fuse layer, Pure rolling + sliding 0,5%

The Figure 18 highlights the different scenarios of microstructure evolution in function of the presence of the run-in or corrosive fuse layer, and thus either in case of pure rolling or rolling with sliding solicitation.

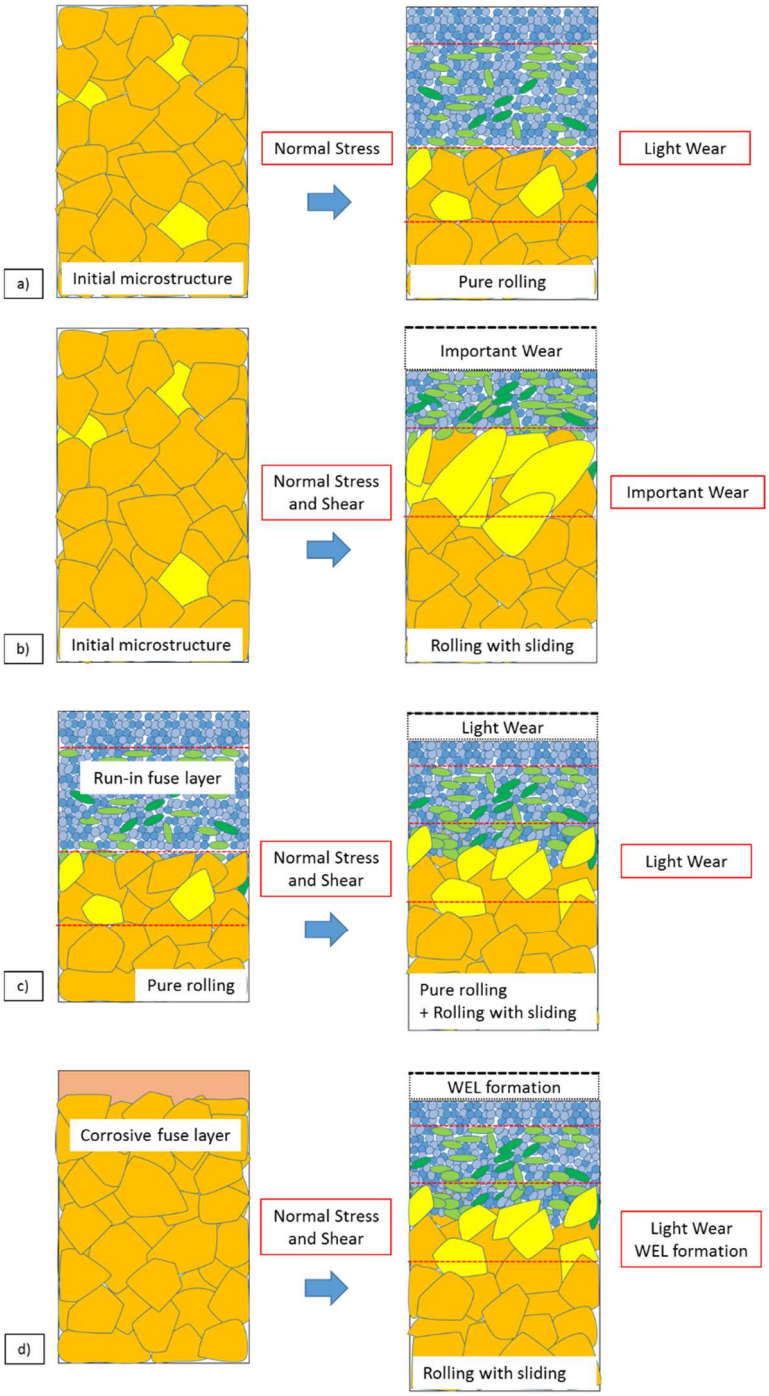

Figure 18 Scenarios of microstructure transformations occurring during (a) Ring B, test #1 and first part of test #3- (b) Ring B, test #2 - (c) Ring B, second part of test #3 - (d) Ring C, test #3. The presence of a nanostructure on the surface (due to run-in fuse layer) limits the wear in presence of shear loading. A corrosive fuse layer enhances the mechanical WEL formation at the surface by the stronger deformation endured by the nanostructural layer, as this latter is protected by the corrosive layer during the first loading cycles

The presence of a fuse layer composed of nanograins (Figure 18(c)), formed during pure rolling (Figure 18(a), reduces the detachment of particles at the surface, as its hardness is higher than the one of the bulk material. Moreover, the deformation gradient increases the cohesion between the top surface and the bulk of the material. This may participate to limit further wear at the surface compared to the same loading applied to plain rail (Figure 18(b)), even when shear is applied, but does not completely prevent it. As a result, the hardened layer slowly vanishes as a result of wear, and do not further deforms. This can explain why no WEL was observed in that case.

By contrast, WEL has developed with the formation of a corrosive layer (Figure 18(d)).
The first reason for this apparition could be a physico-chemical effect: due to carbon and oxygen atoms Chemical affinity, the carbon atoms mobility is reduced, what could change its migration mechanism out of pearlite, and the formation of the WEL is enhanced. This could explain why squats are barely observed in tunnels area where rails are more protected from humidity, and so where corrosion layer are less prone to form [40]–[42].
The second reason could be a kinetic effect, it takes some cycles to completely remove the oxide layer. During this period, the steel sub-layer has time to harden and form a nanograin structure, without being submitted to wear. This nanograin structure sufficiently develops to be further resistant to wear, so that, when submitted to shear stress, it continues to mechanically deform until creating a WEL layer. The formation of mechanical WEL is a progressive process due to the accumulation of solicitations, and a progressive transformation of the microstructure. By contrast, the thermal WEL can be formed very quickly, for instance with a very high sliding ratio. The aspect of the layers observed on the sample with the corrosive fuse layer and a moderate sliding ratio, highly suggests the progressive formation of WEL by spots as presented by (Baumann 1991). Nevertheless the well-known properties of WEL (thermal and mechanical) are established for fully formed and substantial WEL.

5. Conclusions

Tests of rolling contact have been performed on a disc-on-ring test bench. The tests conditions similar to wheel-rail contact, were held in pure rolling and rolling with a realistic sliding ratio. The formation of White Etching Layer (WEL) with a mechanical process was investigated on R260 pearlitic rail steel. The different samples were analyzed through observations of 3rd body flow in the contact, and microstructure characterization of cross-section with optical and scanning electron microscopy (SE and EBSD) and hardness measurements.

The different scenarios of the wear behavior and microstructural transformation were drawn. The influence of the conditions of preparation of the sample surfaces, in particular of the presence of a tribological fuse layer (either a run-in layer or a corrosive layer) on the wear fatigue competition and the WEL formation, were also studied.

The normal stress due to the normal force in the tests leads to the formation of a hardened layer of nanograins. When submitted to shear in the rolling with sliding tests, this layer is removed by wear if the cohesion between the surface and the bulk is too weak. The presence of a fuse layer before the shear solicitation by sliding increases this cohesion, and turns the wear behavior into progressive microstructural transformation. Therefore White Etching Layer were formed through a mechanical process with realistic operating conditions avoiding the formation of thermal WEL.

These results are the key points for the future study of the WEL development during in situ tests. The evolution of the properties of a WEL during its process of formation are less known. At each phase of their development nanohardness tests would be necessary to evaluate the increase of hardness of these WEL spots compared the other points at the sample surface. Further investigations with APT or TEM are required to assess the cementite dissolution which is an indicator of the progression of formation of the mechanical WEL.

Acknowledgments

The authors would like to thank the RATP (Paris Public Transports) (X. Quost S. Simon and P. Boutet) and British Steel (F. Fau and F. Cristofari) for providing the steel samples and founding this study. We also would like to thank E Vittecoq (Hepia Geneva) for the design of the test bench, P. Veuillet, A. Pâquet and D. Leveque for (INSA-Lyon, LaMCoS) for the technical support during the mounting of the bench and the realization of the tests.

[1] X. Deng, Z. Qian, Z. Li, et R. Dollevoet, « Investigation of the formation of corrugation-induced rail squats based on extensive field monitoring », *International Journal of Fatigue*, vol. 112, p. 94‑105, juill. 2018, doi: 10.1016/j.ijfatigue.2018.03.002.

[2] Z. Li, R. Dollevoet, M. Molodova, et X. Zhao, « Squat growth—Some observations and the validation of numerical predictions », *Wear*, vol. 271, nº 1‑2, p. 148‑157, mai 2011, doi: 10.1016/j.wear.2010.10.051.

[3] S. Pal, W. J. T. Daniel, et M. Farjoo, « Early stages of rail squat formation and the role of a white etching layer », *International Journal of Fatigue*, vol. 52, p. 144‑156, juill. 2013, doi: 10.1016/j.ijfatigue.2013.02.016.

[4] M. Steenbergen et R. Dollevoet, « On the mechanism of squat formation on train rails – Part II: Growth », *International Journal of Fatigue*, vol. 47, p. 373‑381, févr. 2013, doi: 10.1016/j.ijfatigue.2012.04.019.

[5] A. Kumar, G. Agarwal, R. Petrov, S. Goto, J. Sietsma, et M. Herbig, « Microstructural evolution of white and brown etching layers in pearlitic rail steels », *Acta Materialia*, vol. 171, p. 48‑64, juin 2019, doi: 10.1016/j.actamat.2019.04.012.

[6] S. Li, J. Wu, R. H. Petrov, Z. Li, R. Dollevoet, et J. Sietsma, « “Brown etching layer”: A possible new insight into the crack initiation of rolling contact fatigue in rail steels? », *Engineering Failure Analysis*, vol. 66, p. 8‑18, août 2016, doi: 10.1016/j.engfailanal.2016.03.019.

[7] G. Baumann, H. J. Fecht, et S. Liebelt, « Formation of white-etching layers on rail treads », *Wear*, vol. 191, nº 1‑2, p. 133‑140, janv. 1996, doi: 10.1016/0043-1648(95)06733-7.

[8] E. Wild, L. Wang, B. Hasse, T. Wroblewski, G. Goerigk, et A. Pyzalla, « Microstructure alterations at the surface of a heavily corrugated rail with strong ripple formation », *Wear*, vol. 254, nº 9, p. 876‑883, mai 2003, doi: 10.1016/S0043-1648(03)00239-4.

[9] R. Nakkalil, « Formation of adiabatic shear bands in eutectoid steels in high strain rate compression », *Acta Metallurgica et Materialia*, vol. 39, nº 11, p. 2553‑2563, nov. 1991, doi: 10.1016/0956-7151(91)90070-H.

[10] H. Blok, « The flash temperature concept », *Wear*, vol. 6, nº 6, p. 483‑494, nov. 1963, doi: 10.1016/0043-1648(63)90283-7.

[11] K. Knothe et S. Liebelt, « Determination of temperatures for sliding contact with applications for wheel-rail systems », *Wear*, vol. 189, nº 1‑2, p. 91‑99, oct. 1995, doi: 10.1016/0043-1648(95)06666-7.

[12] J. Ahlström et B. Karlsson, « Microstructural evaluation and interpretation of the mechanically and thermally affected zone under railway wheel flats », *Wear*, vol. 232, nº 1, p. 1‑14, sept. 1999, doi: 10.1016/S0043-1648(99)00166-0.

[13] J. Wu, R. H. Petrov, M. Naeimi, Z. Li, R. Dollevoet, et J. Sietsma, « Laboratory simulation of martensite formation of white etching layer in rail steel », *International Journal of Fatigue*, vol. 91, p. 11‑20, oct. 2016, doi: 10.1016/j.ijfatigue.2016.05.016.

[14] W. Österle, H. Rooch, A. Pyzalla, et L. Wang, « Investigation of white etching layers on rails by optical microscopy, electron microscopy, X-ray and synchrotron X-ray diffraction », *Materials Science and Engineering: A*, vol. 303, nº 1‑2, p. 150‑157, mai 2001, doi: 10.1016/S0921-5093(00)01842-6.

[15] R. Pan, R. Ren, C. Chen, et X. Zhao, « The microstructure analysis of white etching layer on treads of rails », *Engineering Failure Analysis*, vol. 82, p. 39‑46, déc. 2017, doi: 10.1016/j.engfailanal.2017.06.018.

[16] J. P. Bertrand et J. P. J. Bettembourg, « Phase blanche dans les rails – Caractères métallurgiques et approche mécaniques sur ses conditions de formation », IRSID, Rapport interne MPM 97 N 1126, 1997.
[17] W. Lojkowski, M. Djahanbakhsh, G. Bürkle, S. Gierlotka, W. Zielinski, et H.-J. Fecht, « Nanostructure formation on the surface of railway tracks », *Materials Science and Engineering: A*, vol. 303, nº 1, p. 197‑208, mai 2001, doi: 10.1016/S0921-5093(00)01947-X.
[18] X. Sauvage et Y. Ivanisenko, « The role of carbon segregation on nanocrystallisation of pearlitic steels processed by severe plastic deformation », *J Mater Sci*, vol. 42, nº 5, p. 1615‑1621, mars 2007, doi: 10.1007/s10853-006-0750-z.
[19] S. B. Newcomb et W. M. Stobbs, « A transmission electron microscopy study of the white-etching layer on a rail head », *Materials Science and Engineering*, vol. 66, nº 2, p. 195‑204, sept. 1984, doi: 10.1016/0025-5416(84)90180-0.
[20] S. Simon, A. Saulot, C. Dayot, X. Quost, et Y. Berthier, « Tribological characterization of rail squat defects », *Wear*, vol. 297, nº 1‑2, p. 926‑942, janv. 2013, doi: 10.1016/j.wear.2012.11.011.
[21] L. Wang, A. Pyzalla, W. Stadlbauer, et E. A. Werner, « Microstructure features on rolling surfaces of railway rails subjected to heavy loading », *Materials Science and Engineering: A*, vol. 359, nº 1‑2, p. 31‑43, oct. 2003, doi: 10.1016/S0921-5093(03)00327-7.
[22] L. Beneš, « On wheel–rail contact surface phenomena with structural changes and 'White Etching Layers' generation », *Transport*, vol. 27, nº 2, p. 196‑205, juin 2012, doi: 10.3846/16484142.2012.696214.
[23] H. W. Zhang, S. Ohsaki, S. Mitao, M. Ohnuma, et K. Hono, « Microstructural investigation of white etching layer on pearlite steel rail », *Materials Science and Engineering: A*, vol. 421, nº 1‑2, p. 191‑199, avr. 2006, doi: 10.1016/j.msea.2006.01.033.
[24] R. I. Carroll et J. H. Beynon, « Rolling contact fatigue of white etching layer: Part 1 Crack morphology », p. 14, 2007.
[25] H. Murugan, « Study of White Etching Layer in Rail Steel R260Mn by Thermo-Mechanical Simulation », Delft, 2018.
[26] Y. Zhou, J. F. Peng, Z. P. Luo, B. B. Cao, X. S. Jin, et M. H. Zhu, « Phase and microstructural evolution in white etching layer of a pearlitic steel during rolling–sliding friction », *Wear*, vol. 362‑363, p. 8‑17, sept. 2016, doi: 10.1016/j.wear.2016.05.007.
[27] C. Bernsteiner, G. Müller, A. Meierhofer, K. Six, D. Künstner, et P. Dietmaier, « Development of white etching layers on rails: simulations and experiments », *Wear*, vol. 366‑367, p. 116‑122, nov. 2016, doi: 10.1016/j.wear.2016.03.028.
[28] S. Zitouni *et al.*, « Mechanical conditions and influence of oxidation on White Etching Layers formation », Torino, Italy, 2013, p. 1.
[29] O. Vargolici *et al.*, « Influence of the initial surface state of bodies in contact on the formation of white etching layers under dry sliding conditions », *Wear*, vol. 366‑367, p. 209‑216, nov. 2016, doi: 10.1016/j.wear.2016.06.023.
[30] B. Dylewski, M. Risbet, et S. Bouvier, « Experimental Characterization of the Tridimensional Gradient of Microstructure Induced by RCF in the Rolling Band of Rails », *Procedia Engineering*, vol. 133, p. 202‑210, 2015, doi: 10.1016/j.proeng.2015.12.659.
[31] P. Merino, « Reproduction expérimentale du contact roue-rail à échelle réduite : Voies de formation des sources de défauts », INSA de Lyon, Lyon, 2019.
[32] Y. Berthier *et al.*, « The role and effects of the third body in the wheel–rail interaction », *Fatigue & Fracture of Engineering Materials & Structures*, vol. 27, nº 5, p. 423‑436, avr. 2004, doi: 10.1111/j.1460-2695.2004.00764.x.

[33] A. Saulot, S. Descartes, et Y. Berthier, « Sharp curved track corrugation: From corrugation observed on-site, to corrugation reproduced on simulators », *Tribology International*, vol. 42, nº 11‑12, p. 1691‑1705, déc. 2009, doi: 10.1016/j.triboint.2009.04.042.

[34] *B. Beausir, J.-J. Fundenberger, Analysis Tools for Electron and X-ray diffraction, ATEX - software, www.atex-software.eu, Université de Lorraine - Metz, 2017.* .

[35] C. Kammerhofer, A. Hohenwarter, S. Scheriau, H. P. Brantner, et R. Pippan, « Influence of morphology and structural size on the fracture behavior of a nanostructured pearlitic steel », *Materials Science and Engineering: A*, vol. 585, p. 190‑196, nov. 2013, doi: 10.1016/j.msea.2013.07.032.

[36] P. Ghosh, K. S. Kormout, U. Lienert, J. Keckes, et R. Pippan, « Deformation characteristics of ultrafine grained and nanocrystalline iron and pearlitic steel - An in situ synchrotron investigation », *Acta Materialia*, vol. 160, p. 22‑33, nov. 2018, doi: 10.1016/j.actamat.2018.08.036.

[37] F. Wetscher, A. Vorhauer, R. Stock, et R. Pippan, « Structural refinement of low alloyed steels during severe plastic deformation », *Materials Science and Engineering: A*, vol. 387‑389, p. 809‑816, déc. 2004, doi: 10.1016/j.msea.2004.01.096.

[38] F. Wetscher, R. Pippan, S. Sturm, F. Kauffmann, C. Scheu, et G. Dehm, « TEM investigations of the structural evolution in a pearlitic steel deformed by high-pressure torsion », *Metall and Mat Trans A*, vol. 37, nº 6, p. 1963‑1968, juin 2006, doi: 10.1007/s11661-006-0138-3.

[39] B. Dylewski, « Caractérisation expérimentale multi-échelles et multi-techniques du rail prélevé en service - De la déformation plastique sévère et des évolutions de microstructure à l'amorçage de fissures par Fatigue de Contact de Roulement », UNIVERSITE DE TECHNOLOGIE DE COMPIEGNE, Compiègne, 2016.

[40] S. Simon, « De la dynamique ferroviaire à l'accommodation microstructurale du rail », 2014.

[41] A. Al-Juboori *et al.*, « Evolution of rail surface degradation in the tunnel: The role of water on squat growth under service conditions », *Engineering Fracture Mechanics*, vol. 209, p. 32‑47, mars 2019, doi: 10.1016/j.engfracmech.2019.01.018.

[42] M. Kerr, A. Wilson, et S. Marich, « The epidemiology of squats and related defects », *CORE 2008: Rail; The Core of Integrated Transport*, p. 83, 2008.

[43] Y. Berthier, « Mécanismes et tribologie », 1988.

[44] M. Godet, « The third-body approach: A mechanical view of wear », *Wear*, vol. 100, nº 1‑3, p. 437‑452, déc. 1984, doi: 10.1016/0043-1648(84)90025-5.

[45] V. Linck, « Modélisation numérique temporelle d'un contact frottant - Mise en évidence d'instabilités locales de contact - Conséquences tribologiques », INSA de Lyon, 2005.

ANNEX: Conceptual tools: Third body and flows

In order to describe the different test results, and specifically to take into account the competition between wear and material transformation to form eventually WEL, some conceptual tools will be described.

The tribological triplet introduced by Godet (Godet) is the approach where the two solids in contact (called the “First Bodies”) are separated by a layer of “Third Body”, and are linked by the “Mechanism”. The latter includes the solicitations to the contact, the stiffness and dampers, inertia of the system. The third body is formed from particles of the two first bodies (wheel and rail) but also from external pollution as braking or sand particles, water or leaves for instance on the wheel-rail contact. (Berthier 2004)

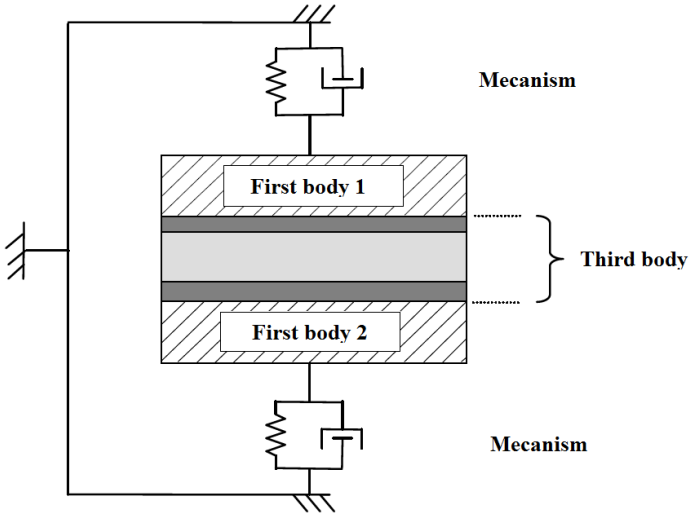

Figure 19 The tribological triplet by Godet and Berthier [43], [44], figure from [45]

A second tool will be used to describe the sample observation, the tribological circuit. It is the material flows in the tribological triplet (Berthier 1988). Five flows are distinguished:

Source Flow Qs: composed of particles detaching from the first bodies staying inside the contact Qsi and the particles coming from the outside of the contact Qse.
Internal Flow Qi: it is the movement of particles within the contact (either inside the third body or the first bodies)
Ejection Flow Qe: it is constituted of particles which are definitely ejected from the contact, wear particles Qw, and particles subjected to go back in the contact later on, the recirculation flow Qr.

These flows can be separated in the lateral and longitudinal directions, and thus are represented for the wheel-rail contact as in Figure 20.

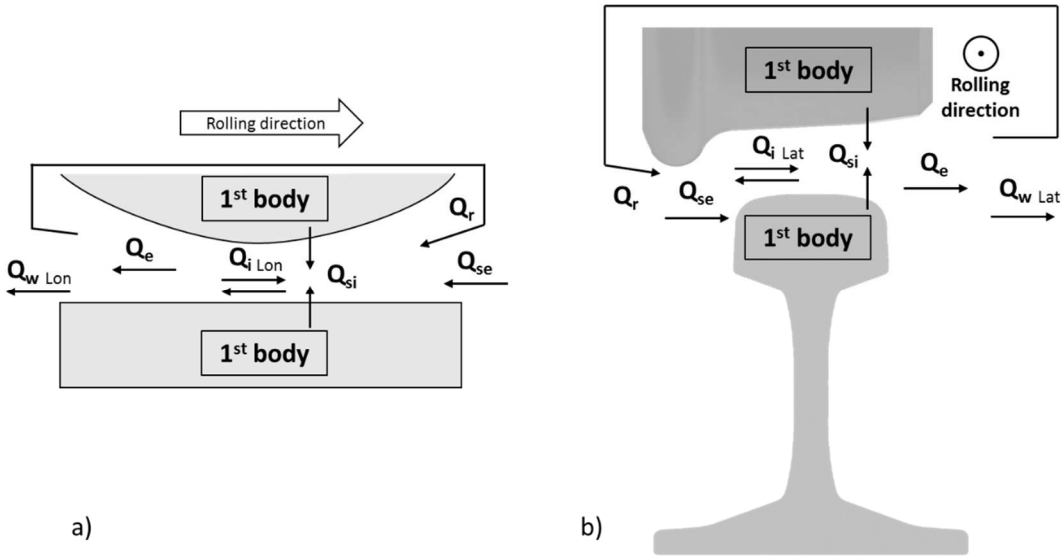

Figure 20 Tribological circuit in wheel-rail contact along a) longitudinal direction, b) lateral direction